Heat and Mass Transfer 38 (2002) 449–457 © Springer-Verlag 2001
DOI 10.1007/s002310100200

Heat and mass transfer characteristics of air bubbles and hot water by direct contact

H. Inaba, S. Aoyama, N. Haruki, A. Horibe, K. Nagayoshi

Abstract This paper has dealt with direct contact heat and mass transfer characteristics of air bubbles in a hot water layer. The experiments were carried out by bubbling air in the hot water layer under some experimental conditions of air flow rate, inlet air temperature and humidity as a dispersion fluid, and hot water temperature and hot water layer depth as a continuous fluid. Heat transfer and evaporation of water vapor from hot water to air bubbles occurred during air bubbles ascending into the hot water. Air bubble flow patterns were classified into three regions of independent air bubble flow, transition and air bubble combination growth. Non-dimensional correlation equations of direct contact heat and mass transfer between air bubbles and hot water were derived by some non-dimensional parameters for three regions of bubble flow pattern.

List of symbols

a	long diameter of ellipsoid bubble, m
A_t	horizontal sectional area of test section, m^2
A_{if}	interface area between air bubbles and hot water, m^2
b	short diameter of ellipsoid bubble, m
C	water vapor concentration
Cp_a	specific heat of dry air at constant pressure, J/(kg K)
Cp_v	specific heat of steam at constant pressure, J/(kg K)
D	diffusion coefficient, m^2/s
d	geometric mean diameter, m
d_m	equivalent diameter of air bubble, m
d_e	hydraulic diameter of wire mesh opening, m
H	height of hot water layer, m
h	specific enthalpy, J/kg
h_l	mass transfer coefficient, m/s
m	mass flow rate, kg/s
m_w	circulating water amount, kg/s
$N \cdot n$	bubble number
Nu	Nusselt number defined by Eq. (9)
P_0	atmospheric pressure, Pa
P_a	saturation water vapor pressure, Pa
P_w	partial pressure of water vapor, Pa
P_{ws}	partial pressure of saturated water vapor, Pa
Pr	Prandtl number
Re	Reynolds number
Q_L	transferred latent heat, W
Q_S	transferred sensible heat, W
Q_T	transferred total heat, W
q_T	total heat flux, W/m^2
r_0	latent heat of vaporization, J/kg
Sc	Schmidt number
Sh	Sherwood number defined by Eq. (15)
T	temperature, °C, K
ΔT	air temperature difference between inlet and outlet of hot water layer, °C, K
U_a	superficial velocity of air flow in the test section, m/s
V	volume flow rate of air, m^3/s
x	absolute humidity

Greek symbols

α	heat transfer coefficient, $W/(m^2\ K)$
ν	kinematic viscosity of air, m^2/s
ϕ	ratio of sensible heat to latent heat
λ	thermal conductivity, W/(m K)

Subscripts

a	air
da	dry air
if	interface
in	inlet
out	outlet
v	water vapor
w	water

Received on 14 July 2000 / Published online: 29 November 2001

H. Inaba (✉), S. Aoyama, N. Haruki, A. Horibe, K. Nagayoshi
Graduate school of Natural Science and Technology
Okayama University, Tsushimanaka 3-1-1
Okayama 700-8530, Japan

1 Introduction

Recently, the direct contact heat transfer method has widely been adopted in many engineering fields by using different heat transfer media like a spray tower for chemical reaction and a cooling tower for cooling [1] etc. The heat transfer medium is made fine and dispersed in the other one for direct contact heat transfer. This fine heat transfer medium results in the expansion of the heating area and reduction in thermal resistance of the heat exchange [2]. As a result, the fineness of the medium provides the increase in the temperature efficiency. In the previous studies [3–5] of direct contact heat transfer by authors, the latent heat storage material at a low melting point in the liquid state was charged into the cold-water layer, and then many fine solid particles of the latent heat storage material were obtained during ascending in the cold-water layer. It was clarified that the effects of various

parameters on the unsteady direct contact heat transfer characteristics between liquid phase and solid phase. On the other hand, the phenomenon of the direct contact heat mass transfer has been applied to obtain the humid air in the air condition's field [2]. Some humidification measures have been used such as the heating of water layer, the natural evaporation from fibers absorbers water, the forced evaporation of fine water droplet to an airflow and direct mixture of the steam to the air [6]. The conventional indoor air-heating system is that the indoor air temperature is raised up by using wall type heat exchanger with the convectional or radiant heat transfer. However, this type heating system results in low relative humidity due to only increase in the indoor air temperature. The present study has proposed the advanced multi-functional heating system in which the low and dry indoor air is heated and humidified at the same time by bubbling the indoor air directly into the hot water layer. Moreover, this direct contact mass transfer between air bubbles and the hot water provides the water filtration function to eliminate dust etc. in the air. The present study has dealt with the direct contact heat and mass transfer characteristics of the ascending air bubbles generated by charging low temperature and humid air in the hot water layer. That is, the present experiments have been done to elucidate the effects of inlet air conditions (air temperature, air humidity and air flow rate) as a dispersion gas phase and hot water conditions (hot water temperature, hot water flow rate) as a continuous liquid phase on direct contact heat and mass transfer characteristics.

2
Experimental apparatus and experimental method

Figure 1 shows the schematic diagram of an experiment apparatus. The experimental apparatus consisted mainly of the test section as direct contact heat and mass transfer exchanger between low-temperature and humidity air bubbles and hot water layer, air quality control system for obtaining low-temperature and humidity air flow, and hot water control system. In the air quality control system, the flow rate pulsation of the air pressurized by the compressor was calmed by using the buffer tank. The air filter was used to eliminate oil droplets from flowing air, which were leaked from the air compressor. The air flow rate in the test section was controlled by the flow-regulating valve, and it was measured with a flow meter (measurement accuracy of $\pm 1.0\%$). The air after measuring flow rate went through the calming section, polymer filter and wire mesh net for air bubble generation, which were mounted on the bottom of the test section. The air bubbles generated from the wire mesh net were heated and humidified during ascending in the hot water layer. Finally, air bubbles were discharged from the test section to the outside. The air pressure in the calming section was measured with the precision pressure gauge (measuring accuracy of ± 0.02 kPa). On the other hand, the hot water temperature was kept at a constant value within ± 0.2 °C at a desired temperature by circulating the hot water from a constant temperature water bath to the test section with an over head tank. The height of hot water layer, H in the test section could be controlled at a given value by adjusting two flow rate control valves that were equipped before and behind the test section. The flow rate of circulating hot water was measured with the orifice type flow meter (measuring accuracy of $\pm 1 \times 10^{-4}$ kg/s).

Figure 2 shows the test section of the direct contact heat and mass exchanger in detail. The test section was constructed by a rectangular vessel (cross section of 100×100 mm, maximum height of 610 mm). The rectangular vessel consisted of the transparent acrylic plate (10 mm in thickness) in order to observe the flow behavior of air bubbles and the hot water. The air calming section

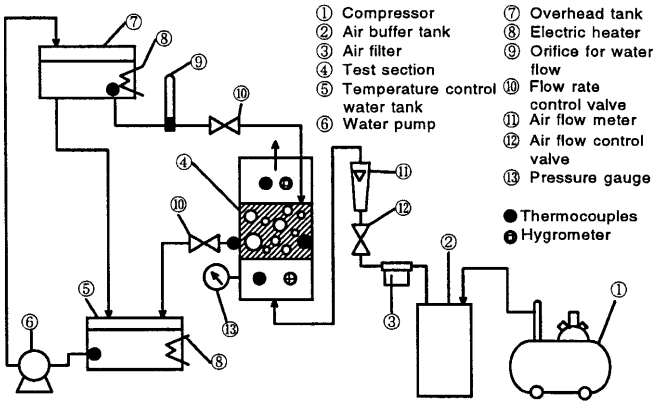

Fig. 1. Schematic diagram of an experiment apparatus

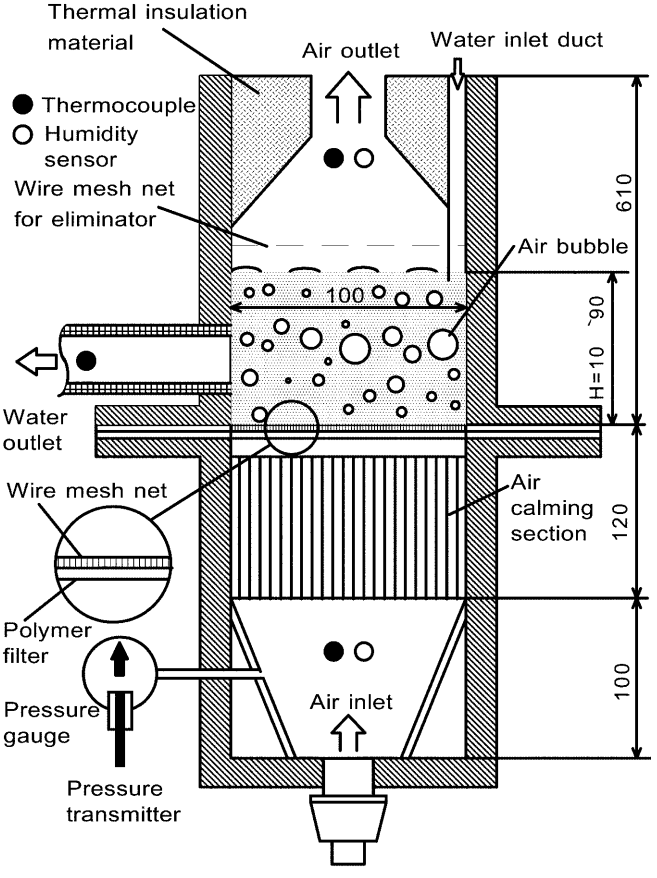

Fig. 2. The test section of the direct contact heat and mass exchanger

under the test section had the dimensions of 100 × 100 mm in section area and 220 mm in height. The expanding section from the pipeline in the length of 100 mm was mounted on the bottom of the air calming section. The air calming section in the height of 220 mm was constructed by the honeycomb structure of 5 mm in square path. The wire mesh net for air bubble generated was mounted on the air calming section. Three kinds of wire meshes (Japan Industrial Standard G 3555) were used, whose mesh dimensions were 30 mesh (aperture of 0.50 mm, wire diameter of 0.34 mm and hydraulic diameter of $d_e = 0.50$ mm), 50 mesh (aperture of 0.30 mm, wire diameter of 0.21 mm and hydraulic diameter of $d_e = 0.30$ mm) and 70 mesh (aperture of 0.212 mm, wire diameter of 0.15 mm and hydraulic diameter of $d_e = 0.212$ mm). Under the wire mesh, the hydrophobic polymer filter (thickness of 0.54 mm, void ratio of 54%) was mounted under the wire mesh net in order to prevent the hot water from leaking. Air inlet temperature (T_{ain}), air outlet temperature (T_{aout}) and hot water temperature (T_w) were measured with the T-type thermocouples (wire diameter of 0.3 mm, measuring accuracy of ±0.05 °C). The measuring position of T_{ain} was located just under the air calming section. The thermocouple for T_{aout} was set into the reduction section made of the thermal insulation material. The wire mesh (100 mesh, apertures of 0.15, wire diameter of 0.10 mm and hydraulic diameter of $d_e = 0.15$ mm) was set between the surface of the hot water and the reduction section. The wire mesh prevented water droplets from adhering to thermocouples and the humidity sensor. The humidity sensors (capacitance type, measuring accuracy of ±1.0%) in order to measure the humidity of the inlet and outlet air were set close to the setting position of the thermocouples. On the other hand, the measuring position for T_w was located out the vertical position of 30 mm from the wire mesh net in the hot water layer. Hot water temperatures at the inlet and outlet of the hot water layer were measured with T-type thermocouples (wire diameter of 0.3 mm, measuring accuracy of ±0.05 °C) as shown in Fig. 2. The experimental condition of hot water flow rate and temperature were decided in consideration of heat and mass supply from the hot water to air bubbles. Figure 3 shows the variation of the heat flux ($q_T = Q_T/A_{if}$), with mass flow rate of the circulating hot water M_v. The value of q_T remains at a constant according to superficial velocity of air flow in the rate of $U_a = 1.3 \times 10^{-2}$–6.3×10^{-2} m/s. The results in Fig. 3 indicate that the heat flux q_T is independent of the hot water flow rate.

The experimental data were obtained under the steady state conditions of heat and mass transfer. The experimental conditions are as follows.

Initial hot water temperature: $T_w = 35.0$–65.0 °C
Hot water level: $H = 10$–90 mm
Superficial air flow velocity: $V_a = 6.4 \times 10^{-5}$–6.3×10^{-4} m^3/s
Air mass flow rate: $m_a = 6.2 \times 10^{-4}$–6.3×10^{-3} kg/s
Inlet air temperature: $T_{ain} = 5.0$–25.0 °C
Absolute humidity of inlet air: $x = 9.0 \times 10^{-4}$–2.0×10^{-3} kg/kg'

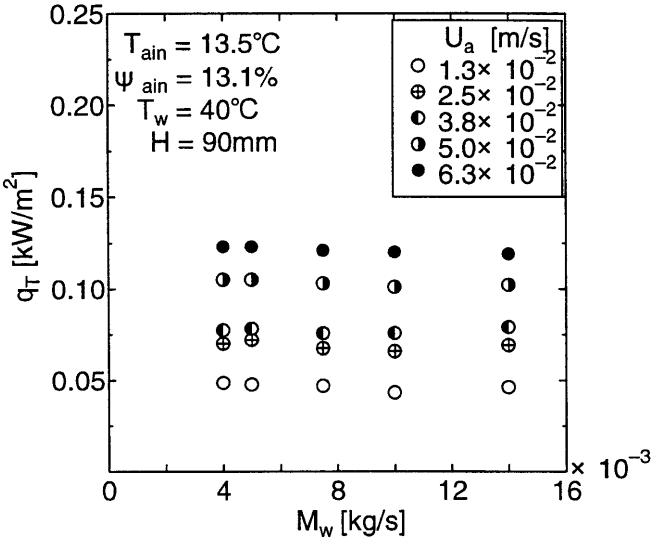

Fig. 3. The variation of the heat flux q_T with mass flow rate of the circulating hot water M_v

3 Experimental results and discussions

3.1 The flow behavior of air bubbles in hot water

In the present study, the wire mesh for generating air bubbles was installed at the bottom of the hot water layer. The diameter of air bubbles was decided within ±0.1 mm by analyzing photographs of flowing air bubbles in the hot water layer. The photographs of flowing air bubbles were taken from the side view of the test section by using high-speed stroboscope with emitted light (light emission time of 1/22,000 s). From the magnified photograph, long diameter (a) and short diameter (b) of air bubbles in ellipsoid shape were calculated by assuming them to form of the rotation ellipsoid. The equivalent diameter of an air bubble was calculated by the following Eq. (1).

$$d_m = \sqrt[3]{\frac{a^2 b}{2}} \tag{1}$$

Mean equivalent diameter d_m of air bubbles was estimated to calculate the arithmetic mean value of about 200 air bubbles from the visualization photograph. Figure 4a–f show the photographs of ascending air bubbles in the hot water layer under the conditions of superficial air flow velocity of $U_a = 6.30 \times 10^{-3}$–$6.28 \times 10^{-2}$ m/s, hot water temperature of $T_w = 40$ °C, inlet air temperature of $T_{ain} = 13.5$ °C and height of the hot water of $H = 90$ mm. Where, superficial air flow velocity in the hot water layer was defined by the superficial velocity whose value was the inlet air volume flow rate divided the horizontal sectional area of the hot water layer. From Fig. 4a, under the condition of the superficial air flow velocity ($U_a = 6.30 \times 10^{-3}$ m/s), it is seen that the air bubbles of mean diameter $d_m = 1$ mm generate from several openings on the wire mesh. The air bubbles can not merge into each other, and they ascend independently in the hot water layer. In Fig. 4a, the air bubbles having large size over

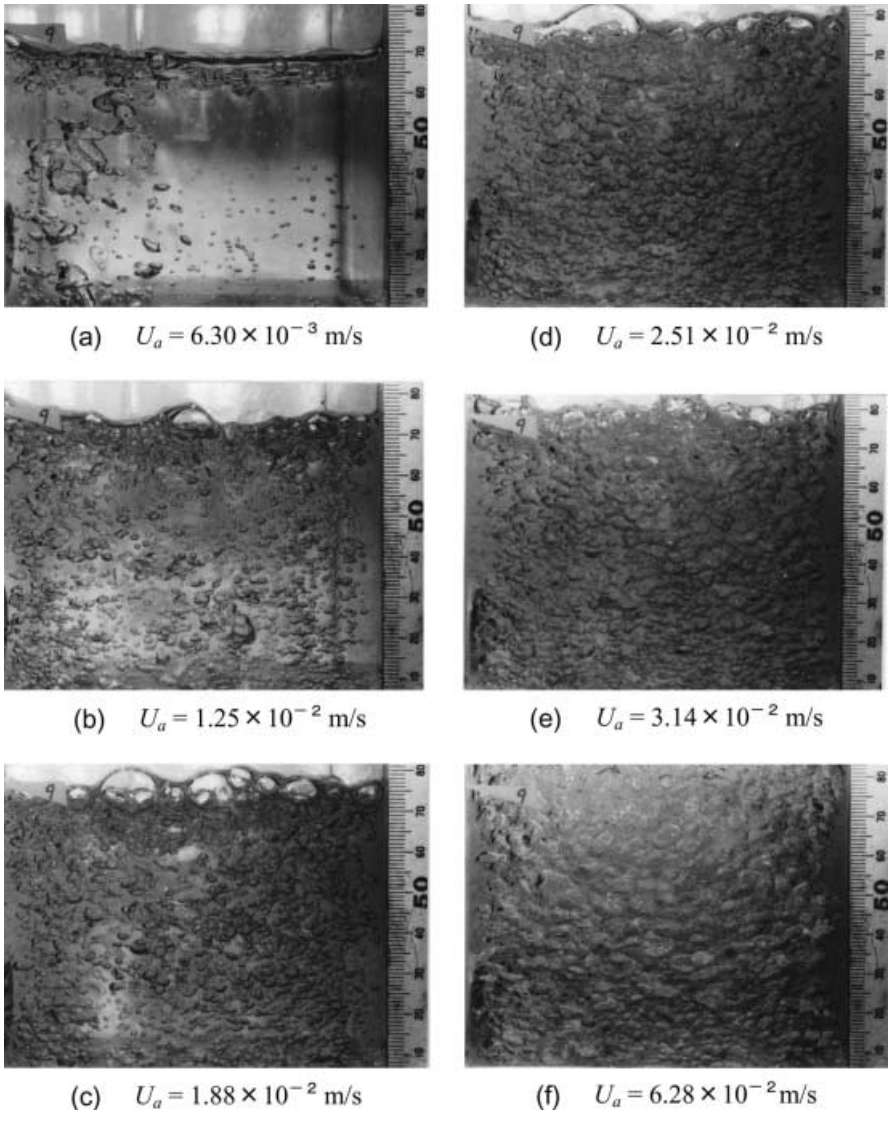

Fig. 4. The photographs of ascending air bubbles in the hot water layer

$d = 10$ mm were also generated. The appearance of these large size air bubbles can be explained as follows. A part of the flow in air was once retained in the gap between the wire mesh and the hydrophobic polymer filter. Subsequently, the new coming air through the polymer filter was supplied to the air gap occupied by the retain air. The pressure of the air gap increased locally, and then the retained air passed the wire mesh. As a result, the large scale air bubbles generated in the hot water layer. In the following evaluation of the air bubble diameter, these large scale air bubbles were excluded in the discussion. As shown in Fig. 4b–c, it is understood that the mean diameter of air bubbles increases up to $d_m = 2$–3 mm with an increase in the superficial air flow velocity, and the ascending velocity of each air bubble also increases. In this superficial air flow velocity range, the generation, the desorption and ascending of air bubbles from the wire mesh were mainly controlled by the buoyancy of air bubbles, etc. In addition, the momentum force of inlet air into the air bubbles just leaving from the wire mesh gradually increases with increasing of the superficial air flow velocity. Consequently, the generation frequency of air bubbles also increases.

In the experimental condition of $U_a \geq 2.51 \times 10^{-2}$ m/s as shown in Fig. 4d–e, the diameter and the density distribution of air bubbles in hot water layer were increased as compared with those in the low air flow velocity range as shown in Fig. 4a–c. Moreover, it is seen that the ascending velocity of air bubbles increases with an increase in inertial force due to the increase in momentum force of inlet air in the high air flow velocity range. However, the generation frequency of air bubbles in the high superficial air flow velocity was lesser than inlet in the low one, since the large scale air bubbles ascended in the central region of the hot water layer. It is seen that the mean diameter of air bubbles decreases with an increase in the superficial air flow velocity. The increase of air bubble density provides the increase in air bubble diameter, due to the combination of air bubbles.

In the experimental condition of superficial air flow velocity over $U_a = 6.28 \times 10^{-2}$ m/s, the complicated circulative flow of the air bubbles was observed as shown in Fig. 4f. A part of air bubbles showed the complicated circulative flow pattern due to the increase in kinetic energy of them. The complicated circulative flow means

that air bubbles stop and descend near the acrylic wall, and then, they ascend again. Moreover, it was observed that air bubbles in the hot water flowed and circulated actively due to the marked separation and combination of air bubbles.

From the measuring results of size and flow behavior of air bubbles, the flow patterns of the air bubbles were classified into following three regions according to superficial air flow velocity U_a.

(1) $U_a \leq 2.5 \times 10^{-2}$ m/s: independent air bubble region
(2) $U_a = 2.5 \times 10^{-2}$–4.0×10^{-2} m/s: transition region
(3) $U_a \geq 4.0 \times 10^{-2}$ m/s: combination and growing air bubble region

Figure 5 shows the relationship between the superficial air flow velocity U_a and geometrical mean diameter d of air bubbles. The geometrical mean diameter d was calculated within ± 0.2 mm by the following Eq. (2). Three kinds of wire meshes for generation of air bubbles were used, such as 30 mesh (hydraulic diameter of $d_e = 0.21$ mm), 50 mesh ($d_e = 0.3$ mm) and 70 mesh ($d_e = 0.212$ mm). In Fig. 5, the lengths of bar lines indicate the measured diameter range of air bubbles, and the open circles show the mean geometrical diameter of air bubbles.

$$d = (d_1 \cdot d_2 \cdots d_n)^{1/n} \tag{2}$$

where, values of $d_1, d_2, \ldots, d_n$ were obtained from Eq. (1) and n means total number of air bubbles in the hot water layer. In this case, the total number of air bubbles n is 200.

As shown in Fig. 5, it is noticed that geometrical mean diameter d increased with an increase in the superficial air flow velocity U_a. In the independent air bubble region ($U_a \leq 2.5 \times 10^{-2}$ m/s), the value of d increases monotonously with increasing U_a. However, in the transition region ($U_a = 2.5 \times 10^{-2}$–4.0×10^{-2} m/s), the increasing rate of d gradually decreases due to the increase in air bubble generation frequency and in coalescence of air bubbles. In the combination and growing air bubble region ($U_a \geq 4.0 \times 10^{-2}$ m/s), the increasing rate of d increases with an increase in the superficial air flow velocity U_a. This phenomenon could be explained by the fact that the coalescence of air bubbles in hot water layer was promoted markedly with increasing kinetic energy of air bubbles.

Figure 6 shows the relationship between the interface area A_{if} of air bubble to the hot water and the superficial air flow velocity U_a. In Fig. 6, the interface area A_{if} was calculated by using Eq. (3) from the geometrical mean diameter d of air bubbles. The uncertainty of the interface area is estimated within ± 0.05 m^2 from the measuring accuracy of the mean geometrical diameter of air bubbles

$$A_{if} = \frac{\pi}{6} d^3 N \tag{3}$$

where, N indicates the total number of air bubbles in the hot water layer. In the independent air bubbles region ($U_a < 4.0 \times 10^{-2}$ m/s), it is seem that the increasing rate of A_{if} increases with increasing the superficial flow velocity U_a, as shown in Fig. 6. However, in the transition region, the increasing rate of A_{if} decreases drastically. On the other hand, the increasing rate of A_{if} to U_a in the combination and growing air bubble region ($U_a > 4.0 \times 10^{-2}$ m/s) was decreased as compared with that in the independent air bubble region ($U_a < 4.0 \times 10^{-2}$ m/s), since the number of air bubbles decreased as a result of the coalescence of air bubbles in the former region.

Figure 7 indicates the relationship between the superficial air flow velocity U_a and holdup ε, which means a volume fraction of air bubbles ascending in the hot water layer. The value of ε was estimated by analyzing the visualization photograph which indicated the variation in the hot water level. From Fig. 7, it is understood that the increasing rate of ε decreases with an increase in U_a. The value of ε was influenced by the buoyancy of air bubbles, surface tension and viscosity of the hot water. It is seen that the increasing rate of ε to U_a decreases with an increase in U_a due to the balance among three factors.

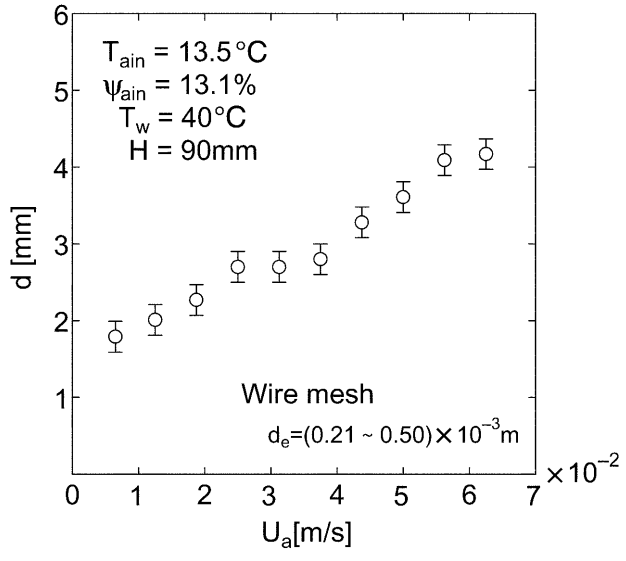

Fig. 5. The relationship between the superficial air flow velocity U_a and geometrical mean diameter d of air bubbles

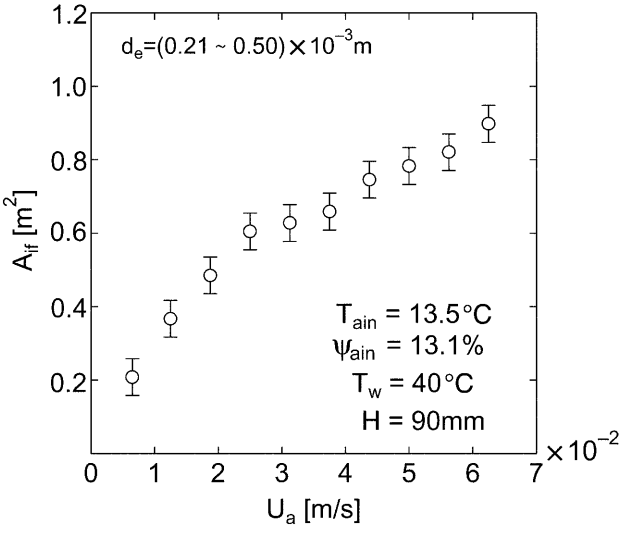

Fig. 6. The relationship between the interface area A_{if} of air bubble to the hot water and the superficial air flow velocity U_a

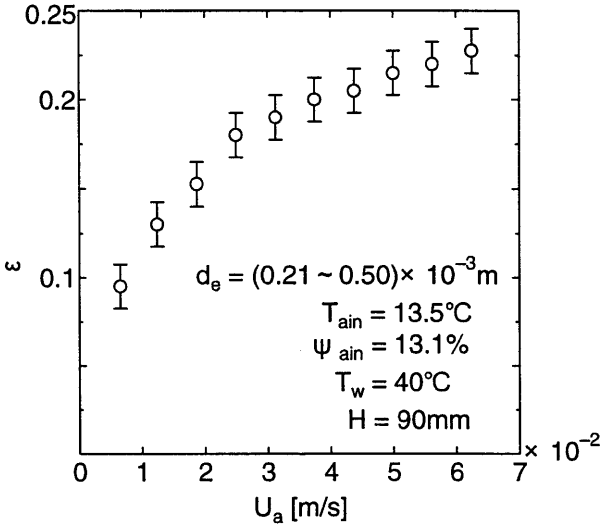

Fig. 7. The relationship between the superficial air flow velocity U_a and holdup ε

3.2 Heat transfer characteristics of air bubbles and the hot water

(a) The calculation method of the heat transfer between air bubbles and the hot water

In this experiment, it is difficult to estimate the transmitted heat from the hot water to air bubbles by using the temperature difference of the hot water that is very small due to the great heat capacity of the hot water as compared with that of air. The total amount of heat transmitted to air bubbles Q_T was estimated from the enthalpy difference between inlet and outlet air of the hot water layer. The specific enthalpy h_{ain} and h_{aout} of inlet air and outlet air, respectively, could be calculated from the relationship between absolute humidity x and air temperature T as shown in the following Eq. (4).

$$h = \{Cp_a T + x(Cp_v T + r_0)\} \tag{4}$$

where, Cp_a and Cp_v refer to the specific heat at constant pressure of dry air and water vapor, respectively. r_0 refers to the latent heat of vaporization at 0 °C. The absolute humidity x of Eq. (4) was calculated by the following Eq. (5)

$$x = 0.622 \times \frac{P_w}{P_0 - P_w} \tag{5}$$

where, P_0 was the atmospheric pressure (=101.325 kPa), and P_w was the partial pressure of water vapor. The value of P_w was derived in terms of the relative humidity $\phi(\%)$ and the saturated water vapor pressure P_s [7] [$P_w = (\phi \cdot P_s)/100$]. Therefore, the total heat Q_T transmitted between the air bubbles and the hot water layer was calculated from the specific enthalpy h_{ain} and h_{aout} of inlet air and outlet air, respectively by using the following Eq. (6)

$$Q_T = \frac{m_{ain}}{1 + x_{ain}}(h_{aout} - h_{ain}) \tag{6}$$

where, m_{ain} refers to the mass flow rate of inlet air. The total heat Q_T depends on the uncertainties of the temperature, pressure and mass flow rate measurements; it is estimated within 1.0 W.

(b) The effect of the hot water layer on the heat flux

Figure 8 shows the relationship between the heat flux q_T ($=Q_T/A_{if}$) and the hot water layer height H. From Fig. 8, it is seen that the hot water layer height H in this experiment range ($H = 1$–9×10^{-2} m) does not exert an influence on the total heat transmitted Q_T, so that the heat flux q_T was almost constant in every superficial air flow velocity U_a. From this results, it is understood that the heat and mass transfer from the hot water to air bubbles are completed for a short time when air bubbles ascend in the hot water layer. On the other hand, it is noticed that the heat flux q_T increases with an increase in the superficial air flow velocity U_a since the turbulence intensity of hot water flow induced by air bubble moment and the interface area of air bubbles are increased with increasing U_a.

(c) The effect of the superficial air flow velocity on the heat flux

Figure 9 shows the relationship between the heat flux q_T and the superficial air flow velocity U_a for various hot water temperatures T_w, under experimental conditions of $T_{ain} = 12.2$–16.5 °C, $\phi_{in} = 12.8$–14.0% and $H = 0.09$ m. The results of Fig. 9 indicate that the heat flux q_T increases with an increase in the superficial air flow in the independent air bubbles region, however, the increasing rate of q_T decreases in the transition region, while the value of q_T increases again in the combination and growing air bubble region. These results could be explained as follows. The total amount of heat Q_T transferred between the hot water and air bubbles is estimated by summing up sensible heat Q_S by convective heat transfer and latent heat Q_L by vaporization of hot water. The latent heat Q_L that occupied most of the total heat Q_T is obtained by the product of the

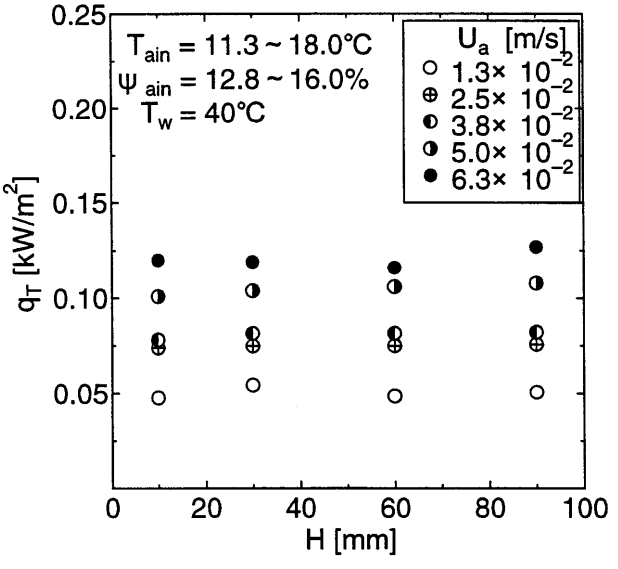

Fig. 8. The relationship between the heat flux q_T ($=Q_T/A_{if}$) and the hot water layer height H

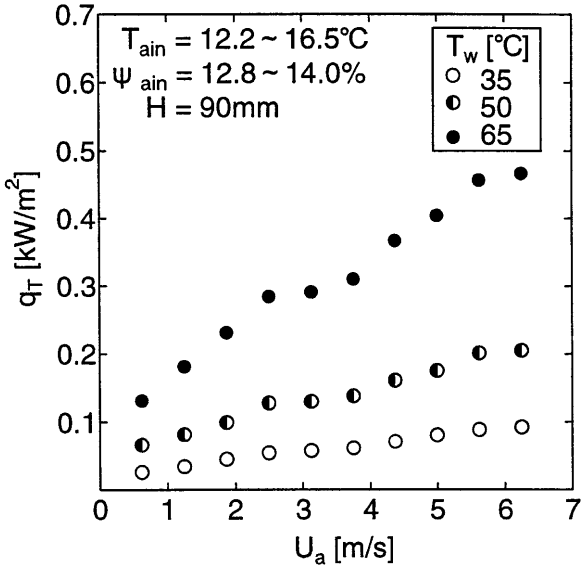

Fig. 9. The relationship between the heat flux q_T and the superficial air flow velocity U_a for various hot water temperatures T_w

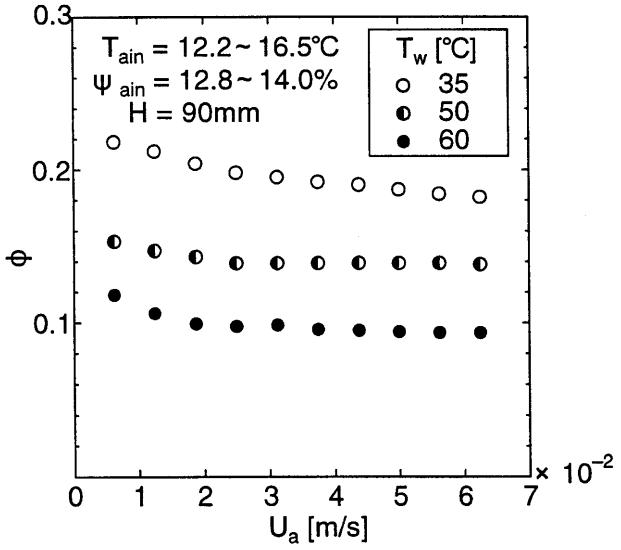

Fig. 10. The relationship between the ratio of sensible heat to latent heat ϕ and the superficial air flow velocity U_a

latent heat of water vaporization r at the interface temperature and water vapor mass m_w which generates from the interface between air bubbles and the hot water. This water vapor mass m_w is dependent on the concentration difference of water vapor between the interface and air bubbles. The saturated water vapor concentration at the interface increased exponentially with an increase in the interface temperature, that is, the hot water temperature T_w in the high temperature region. Therefore, latent heat Q_L as well as water vapor m_w increases with increasing the vapor concentration difference between them. As the result, the heat flux q_T consequently increases with an increase in the hot water temperature.

The sensible heat Q_S transferred from the hot water to air bubbles are calculated by the following Eq. (7).

$$Q_S = Cp_a \cdot \Delta T \cdot m_{dain} + Cp_v \cdot \Delta T \cdot m_{vin} \qquad (7)$$

where, Cp_a and Cp_v refer to specific heat at constant pressure of dry air and water vapor, respectively, ΔT is the temperature difference between inlet and outlet air, and m_{dain} and m_{vin} pertain to mass concentration of dry air and water vapor of inlet air, respectively. The sensible heat Q_T is estimated by the uncertainty of the measuring accuracy of the temperature and the mass concentration. As a result, the uncertainty of the sensible heat is within 1.0 W.

Figure 10 shows the relationship between the ratio of sensible heat to latent heat ϕ ($=Q_S/Q_L$) and the superficial air flow velocity U_a. In the present experimental condition, it is seen that most of total heat transmitted is dependent on the latent heat of vaporization due to the low value of ϕ. It is understood that the increase in T_w is allowed to prompt the latent heat of evaporation, that is, to reduce the value of ϕ.

Figure 11 indicates the variation of heat transfer coefficient α with the superficial air flow velocity U_a for various hot water temperatures T_w under the same experimental conditions as mentioned in Fig. 9. The heat transfer

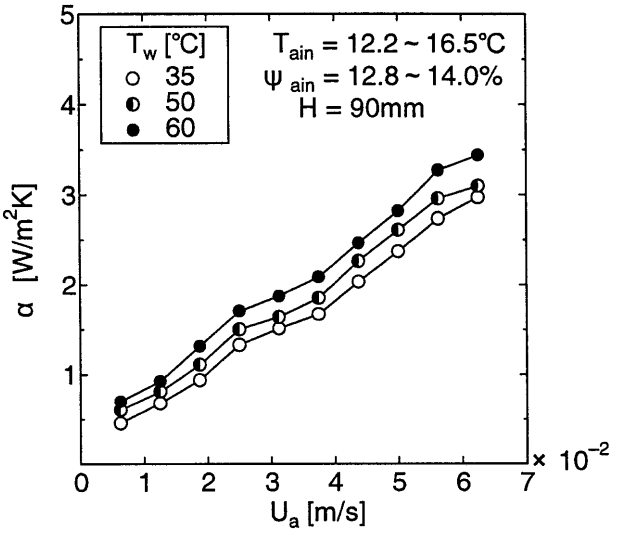

Fig. 11. The variation of heat transfer coefficient α with the superficial air flow velocity U_a for various hot water temperatures T_w

coefficient α is defined as follow. The uncertainty of α depends on the uncertainty of the sensible heat Q_S and the temperature measurements. The uncertainty of the heat transfer coefficient is within ± 0.05 W/(m^2 K).

$$\alpha = \frac{Q_S}{A_{if}(T_{aout} - T_{ain}) / \ln\{(T_w - T_{ain})/(T_w - T_{aout})\}} \qquad (8)$$

As shown in Fig. 11, it is seen that the value of α increases with increasing U_a, however, the increasing rate of α to U_a is different according to each air bubble flow pattern, like in the independent air bubbles region, the transition region and the combination and growing air bubble region. The increase in α is contributed to the increase in Prandtl number in relation to the rise in hot water temperature.

The data of Nusselt number Nu, which expresses the non-dimensional heat transfer, against Reynolds number Re are plotted in Fig. 12, where Nusselt number Nu and Reynolds number Re are defined as follows. The relative uncertainties of Nu and Re are estimated to be ±7.0 and ±5.0%, respectively from the measuring accuracies of the heat transfer coefficient α and the superficial velocity of air flow in the test section U_a.

$$\mathrm{Nu} = \frac{\alpha \cdot d}{\lambda}, \quad \mathrm{Re} = \frac{U_a \cdot d}{\nu} \tag{9}$$

In each air bubble flow region, Least-squares fitting method is applied to the obtained data reduction. Nusselt number is derived as a function of Reynolds number and Prandtl number with the standard deviation of ±9.5% as follows.

- Independent air bubble region ($0.75 \leq \mathrm{Re} \leq 2$):

$$\mathrm{Nu} = 0.0539\,\mathrm{Pr}^{\frac{1}{3}}\mathrm{Re}^{0.748} \tag{10}$$

- Transition region ($2 < \mathrm{Re} < 7$):

$$\mathrm{Nu} = 0.0886\,\mathrm{Pr}^{\frac{1}{3}}\mathrm{Re}^{0.463} \tag{11}$$

- Combination and growing air bubble region ($7 \leq \mathrm{Re} \leq 18$):

$$\mathrm{Nu} = 0.0343\,\mathrm{Pr}^{\frac{1}{3}}\mathrm{Re}^{0.984} \tag{12}$$

The results of these experimental correlation equations reveal that the index number 0.748 of Re in Eq. (10) is greater than of 1/2 in a common laminar convection heat transfer around a solid body due to the deformation and turbulence of air bubbles. While it is seen that the index number of Re, 0.984 in Eq. (12) is also greater than that of 0.8 in a common turbulent convection heat transfer around the solid body since the strong turbulent circulation flows of air bubbles and hot water appear in the hot water layer.

3.3
Mass transfer characteristics between air bubbles and the hot water layer

As shown in Fig. 10, the latent heat of evaporation occupies more than 80–90% of total heat transmitted from hot water to air bubbles in the present experiment conditions. In this present study, mass transfer on the interface between air bubbles and hot water is non-dimensionalized in consideration of the water vapor diffusion phenomenon induced by water vapor concentration difference between the interface of air bubbles and inside of air bubbles. The mass transfer coefficient h_l is defined by the following Eq. (13). The uncertainty of the mass transfer coefficient depends on the uncertainties of the total amount of heat

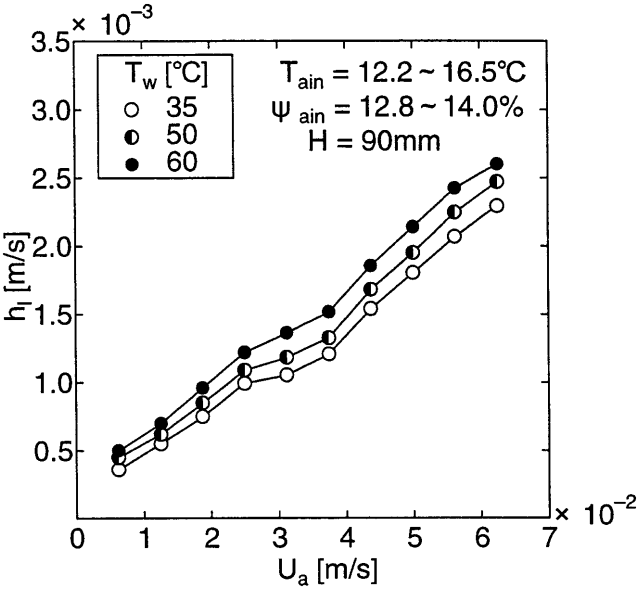

Fig. 13. The relationship between the mass transfer coefficient h_l and the superficial air flow velocity U_a

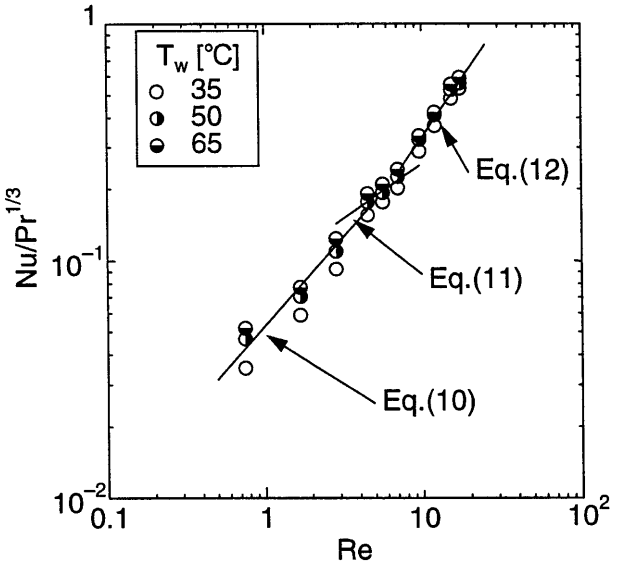

Fig. 12. The relationship between the non-dimensional heat transfer, $\mathrm{Nu/Pr}^{1/3}$, and Reynolds number Re

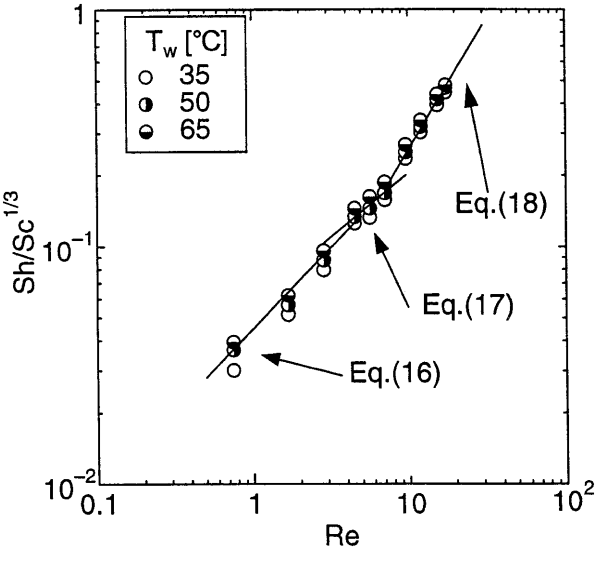

Fig. 14. The variation of Sherwood number $\mathrm{Sh/Sc}^{1/3}$ with Reynolds number Re

transmitted to air bubbles and the water vapor concentration; it is estimated within ±0.05 m/s.

$$h_l = \frac{Q_T}{A_{if}\Delta C} \tag{13}$$

where, ΔC refers to the logarithmic mean water vapor concentration difference as follows.

$$\Delta C = \frac{C_{aout} - C_{ain}}{\ln\{(C_{iv} - C_{ain})/(C_{iv} - C_{aout})\}} \tag{14}$$

where, C_{ain}, C_{aout} and C_{iv} correspond to water vapor concentrations of inlet air and outlet air and the saturated water vapor, respectively. In the present study, C_{iv} is assumed as the saturated water vapor concentration at hot water temperature. Figure 13 shows the relationship between the mass transfer coefficient h_l and the superficial air flow velocity U_a. In Fig. 13, it is understood that the value of h_l increases with an increase in U_a, and the increasing rate of h_l to U_a is different in each air bubble flow region as mentioned above in the discussion of the heat transfer coefficient. Moreover, it is noticed that the increasing rate of h_l to U_a decreases with increasing the hot water temperature T_w, since the water vapor concentration boundary layer thickness of the air developed on the interface is reduced with an increase in T_w. As a result, the reduction in vapor concentration boundary layer thickness results in the promotion of mass transfer.

Figure 14 shows the variation of Sherwood number Sh/$Sc^{1/3}$, which means the non-dimensional mass transfer coefficient, with Reynolds number Re. The Sherwood number Sh is defined as follows.

$$Sh = \frac{h_l d}{D} \tag{15}$$

where, D is the diffusion coefficient of vapor to air. The relative uncertainty of Sh is estimated by the uncertainty of the mass transfer coefficient. As a result, it is within ±6.0%. From Fig. 14, it is noticed that the value of Sh increases with an increase in Re, and the increasing rate of Sh to Re is different in each of three air bubble flow regions. By the least squares fitting, the experiment correlations of Sherwood number Sh are derived by means of Re and Sc, with the relative error of ±5.0%.

- Independent air bubbles region ($0.75 \leq Re \leq 2$):

$$Sh = 0.0419\, Sc^{\frac{1}{3}} Re^{0.685} \tag{16}$$

- Transition region ($2 < Re < 7$):

$$Sh = 0.0587\, Sc^{\frac{1}{3}} Re^{0.541} \tag{17}$$

- Combination and growing air bubble region ($7 \leq Re \leq 18$):

$$Sh = 0.0203\, Sc^{\frac{1}{3}} Re^{1.10} \tag{18}$$

where, Sc refers to the Schmidt number of air.

4 Conclusions

The effect of some parameters on the direct contact heat and mass transfer characteristics of air bubbles in touch with the hot water layer was examined experimentally by generating air bubbles into the hot water layer through the wire mesh net. The following conclusions were obtained.

(1) The mean diameter of air bubbles generated through the wire mesh net increased with an increase in the superficial air flow velocity. And, the air bubble flow pattern was classified into three regions of the independent air bubble region in which air bubbles ascended independently, the transition region and the combination and growing air bubble region in which air bubbles were disunited and united each other.

(2) It was seen that the heat and mass had been transferred from the hot water to air bubbles for a very short time when air bubbles were left from the wire mesh net, and the water level of the hot water layer did not exert an influence on the heat and mass transfer characteristics of air bubbles.

(3) With regard to the heat and mass transfer between air bubbles and the hot water, it was clarified that the increasing rates of the heat and mass transfer coefficient varied according to the three air bubble flow patterns depending on the superficial air flow velocity.

(4) The non-dimensional correlation equations of the heat and mass transfer between air bubbles and the hot water were derived in terms of Reynolds number and Prandtl number or Schmidt number.

References

1. **The Japan Society of Mechanical Engineers** (1996) JSME STANDARD Standard Method for Heat Exchanger Thermal Design (JSME S011), The Japan Society of Mechanical Engineers: Maruzen, pp. 110–116
2. **Frank Kreith; Boehm RF** (1988) Direct Contact Heat Transfer, Springer-Verlag, Berlin, p. 343
3. **Inaba H; Sato K** (1994) Fundamental study on latent cold heat storage by means of oil droplets with low freezing point (1st Report, Flow and Solidification Characteristics of Tetradecane Droplets Ascending in Low-Temperature Water Solution). Trans JSME (B) 60(580): 4236–4243
4. **Inaba H; Sato K** (1996) Fundamental study on latent cold heat storage by means of oil droplets with low freezing point (2nd Report, Nondimensional Analysis of Solidification and Heat Transfer Characteristics of Tetradecane Oil Droplets Ascending in Low-Temperature Water Solution). Trans JSME (B) 62(593): 325–332
5. **Inaba H; Sato K** (1997) Fundamental study on latent cold heat storage by means of oil droplets with low freezing point (4th Report, Numerical Calculation of Motion and Solidification Characteristics of Oil Droplet Ascending in a Cold Water Solution by Buoyancy). Trans JSME (B) 63(607): 1021–1028
6. **Japanese Association of Refrigeration** (1993) JAR Handbook 5th Edition Equipments, Japanese Association of Refrigeration, Japan, pp. 432–435
7. **Tanishita I** (1989) Thermodynamics, Shokabo Pub. Co., Japan, pp. 233–234